Research on Engineering Structures & Materials

www.jresm.org

Research Group

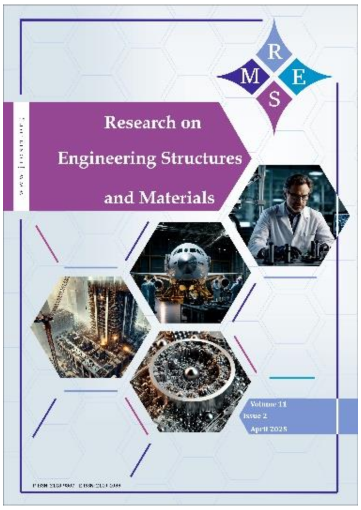

Using a non-homogeneous Markov Model to predict the load-deflection curve of concrete-encased steel I-beams

Tamara Adnan Qasim

Online Publication Date: 10 July 2026

URL: http://www.jresm.org/archive/resm2026-1636st0424rs.html
DOI: http://dx.doi.org/10.17515/resm2026-1636st0424rs

Journal Abbreviation: *Res. Eng. Struct. Mater.*

To cite this article
Qasim T A. Using a non-homogeneous Markov Model to predict the load-deflection curve of concrete-encased steel I-beams. *Res. Eng. Struct. Mater.*, 2026; 12(4): 3041-3057

Research on Engineering Structures & Materials
www.jresm.org
MIM Research Group

Research Article

Using a non-homogeneous Markov Model to predict the load-deflection curve of concrete-encased steel I-beams

Tamara Adnan Qasim [*,a]

Department of Civil Engineering, College of Engineering, Al-Iraqia University, Baghdad, 10071, Iraq

Article Info

Article History:

Received 24 Apr 2026

Accepted 07 July 2026

Keywords:

Markov Chain;
I-section steel;
Closed beam;
Reinforced concrete;
Estimate curve load-deflection

Abstract

A non-homogeneous Markov chain framework predicts the load-deflection curve in relation to different loads and deflections for the beams being tested. The load–deflection response was modeled using six discrete load levels and seven deflection states, where the deflection at midspan (discrete-state) can occur in a defined range or "delta c" (minimum to maximum). The transition matrices are derived from characteristics of the specimen beams (using ACI and AISC) and from the experimental measurement of the epochal test results of load and deflections, along with the associated time sequences through the "Markov" model. Incremental deflection was modeled using a normal distribution as a simplifying probabilistic assumption to estimate transition probabilities between discrete deflection states. Furthermore, the distribution has been evaluated by analyzing the mean-square-error (MSE). Two specimen beams were included in the evaluation (C1 and C2), and the performance was assessed using root mean square error (RMSE), normalized root mean square error (NRMSE), mean absolute percentage error (MAPE), accuracy acceptance (AA), coefficient of determination (R^2), and Pearson correlation coefficient (Pearson R). Beam C1 RMSE was 3.03 mm, AA = 97.62%, and R^2 = 0.9920. Beam C2 RMSE was 6.64 mm, AA = 93.03%, and R^2 = 0.9783. Within the proposed Markov framework, failure probability is defined as the probability that the beam reaches the terminal deflection state associated with a predefined limit state.

1. Introduction

Composite steel–concrete structural systems exhibit significant structural advantages when the steel section is encased in or connected to concrete, allowing both materials to act together under applied loading. The structural performance of composite steel and concrete structural systems can also be considered. Composite members include steel 'I' sections, as well as other structural members, encased and/or connected to concrete and allowing for the materials to work together and respond to the applied load jointly. The combination of steel and concrete results in a high-performance structural system, leveraging the strengths of both materials. Steel is primarily known for its advantageous tensile strength and, more importantly, ductility. In contrast, concrete is mainly known for its compressive resistance and stiffness [1-3]. When properly bonded, steel and concrete working together to form an effective composite structural system, which will be discussed shortly. The outcome is a more, ductile, energy-efficient and effective structure. In structural engineering practice, the metals and the cementitious family, steel and concrete, respectively, the load-deflection behavior of steel–concrete composite sections is significantly influenced by the shear connection and the degree of composite interaction between the steel section and the surrounding concrete [4].

*Corresponding author: t.adnan82@aliraqia.edu.iq
[a]orcid.org/0000-0002-9736-7217
DOI: http://dx.doi.org/10.17515/resm2026-1636st0424rs

Understanding serviceability and failure mechanisms in composite beams necessitates a well-characterized load-deflection curve. It has been shown that the composite I-beam stiffness and deflection characteristics are sensitive to longitudinal reinforcement, degree of composite action, and concrete confinement by several researchers [5-7]. Traditional methods for estimating deflection, such as differential equations of elastic behavior and finite element analysis, are useful for deterministic response prediction. The majority of traditional methods generate a single response curve using fixed properties of the material, fixed boundary condition, and fixed load assumption. It may be possible to define the relationship between the increasing load on the structure and the transition between ranges of deflection; however, these methods do not quantify the uncertainty associated with cracks, loss of stiffness and the variability between specimens. Therefore a Markov chain is established as the model to represent the load–deflection relationship as a series of probabilistic transitions through discrete states of deflection [8].

The Markov chain model has recently been used to evaluate parameters such as the life expectancy of a building, how far a crack will spread, and its reliability. The Markov chain model belongs to a larger group of models called stochastic models, which use probability and statistical methods to predict future behaviors. In the case of the Markov chain model, the future behavior is predicted by looking at previous behaviors or changes among different states of a system. These different states must be defined and fixed to different parts of the system. Once these rules are set they will not change from there on. The Markov chain model evaluates the changes of a system's state in a given time and records the result [9,10]. The Markov model has been used extensively in modeling the detailed actual load-deflection behavior of composite I-beams consisting of steel and concrete. Most of the work until now concentrated either on deterministic models or probabilistic deterioration under long-term environmental exposure [11,12]. The discrete state transitions to capture the progressive deflection behavior of steel-concrete composite beams under monotonic or incremental loading have not been sufficiently addressed [13].

An approach for estimating the monotonic load-deflection behaviour of encased composite beams has been developed as a Markov chain-based stochastic model. The primary basis for this approach is to model structural responses as a sequence of discrete deflected states (i.e., deflection state transitions associated with given incremental load steps) in which the current state of the structure and the magnitude of the applied incremental loading control the probability of transitioning from the currently observed state to another state in the subsequent incremental loading. While probabilistic structural models have been successfully employed for assessing both time-dependent degradation of structures and time-dependent reliability of structural components, their application to predicting response curves (i.e., developing a continuous load-deflection response over the entire range of increasing loads on a monotonically loaded structure) is limited, particularly with respect to encased composite structures. This limitation is significant because the traditional code-based methods for determining monotonic load-deflection responses (e.g., ACI and AISC sectional equations) are based on particular assumptions regarding the behavior of the structure during load application and only provide point estimate response curves; therefore, they do not provide any indication of the uncertainty or variability in the evolving structure due to stiffness degradation throughout the allocated timeframe of a structural component. A Markov-based model has been developed for predicting the load-deflection curve from the transition structure learned from the averages of the responses generated by the ACI and AISC equations, providing an additional "simplified" probabilistic approximation to non-linear stiffness evolution using a discrete data set that may still be used in conjunction with existing code based mechanics.

Most previous studies on the behavior of steel-concrete composite beams mainly relied on either deterministic analytical models or the more detailed representation provided by finite element (FE) analyses. While unimodal analytical models provide detailed local responses, they are computationally expensive when performing the progressive transition between deflection states, FE analysis does not capture the probability associated with transitioning from one deflection state to another. Thus, this study fills a gap in the literature whereby no simple, probabilistic framework has been developed to track the progressive load-deflection response of concrete encased steel I-beams under monotonic loading and express uncertainty regarding deflection state transitions. A Markov-chain model has been proposed to provide a solution to this gap by transforming the load-deflection response into a series of discrete probabilistic states such that the model may predict the probability of transitioning from one deflection state to another, as load is increased.

2. Materials and Sample Preparation

An attempt was made to assess the accuracy and predictability of the proposed model against two other existing models that have been subjected to experimentation. Previous experimental evaluations conducted by Xian et al. [14] and Mahmood [15] were performed using two individual concrete-encased composite beams (i.e., Case C1 and Case C2) in a flexural test when a single point load was applied at mid-span along a simply supported beam placed in a monotonic, three-point bending configuration. Clear spans were equal to 2,000 mm for Beam C1 and 2,750 mm for Beam C2, which is the reason for differentiating between how these two experiments were referenced in this study. For beam C1, the spans of the supports were 2000 mm, while those for beam C2 were 2750 mm. The works reported by these authors will be referred to as Case C1 (for beam C1) and Case C2 (for beam C2).

The C1 beam tested by Xian et al. has a concrete cross-section of 160 mm × 250 mm. The C1 beam includes a steel profile with a height of 140mm; it has a web with a thickness of 5.5mm and flanges 80 mm wide x 9.1 mm thick. The concrete was reinforced with a 40 mm overlay of concrete rebar over the top and bottom of the beam, the top rebar having an area of 85 mm^2 and a bottom rebar area of 57mm^2. The C1 beam had a total span of 2000 mm with a shear span of 120mm (0.12m). The concrete had a compressive strength of 48.4MPa, tensile strength of 4.8 MPa, and elastic modulus of 33.23GPa. The assumed ultimate strain at failure is 0.002*, and the cracking strain is 0.0004*. The yield strength of the reinforcing steel is 276 MPa, the elastic modulus is 200 GPa; whereas the yield strength of the steel profile is 315 MPa and the ultimate strength is 410 MPa. Parameters identified with an asterisk (*) were not reported directly from the original source required for analytical purposes; however, the following values referenced below are from related design codes or literature in support of other similar steel/concrete composite elements. No unmarked estimated values were included in the analysis.

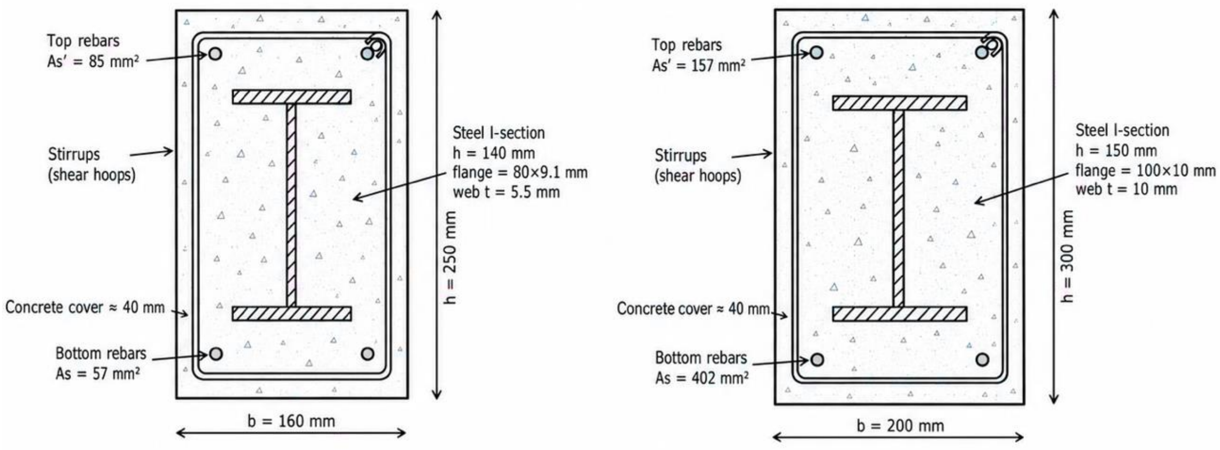

Fig. 1. Cross-section details and three-point bending configuration of Beams C1 and C2

By comparison, C2 from Mahmood et al. section with dimensions of 200 mm × 300 mm and a steel section 150 mm high, 10 mm thick web and 100 mm broad flanges with 10 mm thick flanges, reinforced with 40 mm of concrete and a much larger area for reinforcement than for its counterpart. In addition to the larger area (157 mm^2 and 402 mm^2 for tension and compression, respectively), the span length is 2750 mm, and the shear span is 150 mm. The compressive strength of concrete was lower (25.75 MPa), and the tensile strength (2.78 MPa) and elasticity (23.98 GPa) of concrete were lower than in Beam C1. The strain at cracking was significantly greater (0.004) than in C1. Beam C2 has a yield strength of 520.7 MPa of reinforcing steel (in the original experimental source of 600 MPa ultimate strength) as being unique for C2. The constituent materials for C2 are not characterized as similar to those in C1 (the yield and ultimate strength for C1 are still 315 and 410, respectively).

To clarify, Beam C1 was simply Supported three-point bending conditions with a concentrated load applied at midspan and a clear support span of 2000 mm. The same was true for Beam C2 but the point load was at the midpoint and had 2750mm between the supports. The attached schematic includes the cross-section and loading configuration for both Beam C1 and C2 together with details of concrete dimensions, concrete covering, embedded steel I-section, stirrups, and reinforcement position. The parameters denoted by an asterisk (*) were either unreported in the original experimental source or were simply extrapolated from design code recommendations or literature on comparable-sized steel-concrete composite structural members. Only those parameter values that were required for analytical purposes were utilized; no estimates (unmarked parameters) were included in the analytical calculation.

3. Markov Chain Modeling and Code Integration (ACI & AISC)

When reinforced concrete beams designed to be nominally identical are subjected to monotonically increasing loads, their load–deflection responses exhibit noticeable variability between specimens. This variation, illustrated in Figure 2, reflects the stochastic nature of the deflection behavior, which is referred to as the "deflection process" in this study. Incremental deflections between subsequent load levels are controlled by the normal distribution assumption. The normal distribution assumption provides a reasonable probabilistic representation of incremental deflections, where transition probabilities for each load step are estimated using the deflection mean and standard deviation. While the normal distribution assumption simplifies the evaluation, it does not accurately represent highly nonlinear response phases where deflections might be skewed. Therefore, any interpretation of the results will be dependent upon the calibrated limits of each tested beam. The deflection process is represented as (y max.L, L belongs to Z). For each load L belongs to Z, the maximum deflection, y maxL. At each load level L, the corresponding maximum mid-span deflection y maxL is treated as a random variable. The index set Z defines the sequence of load applications, while the deflection state space consists of all possible values that ymaxL may assume [9,11]. The state space for modeling can be divided by defining a finite range for each resulting deflection state, since the ability of the states to be defined on a continuum or on a discrete set of values is a consequence of the process index. The deflection is therefore a discrete stochastic process and the beam itself is the system, where, at any load level, the state of the system is defined by the maximum deflection [10].

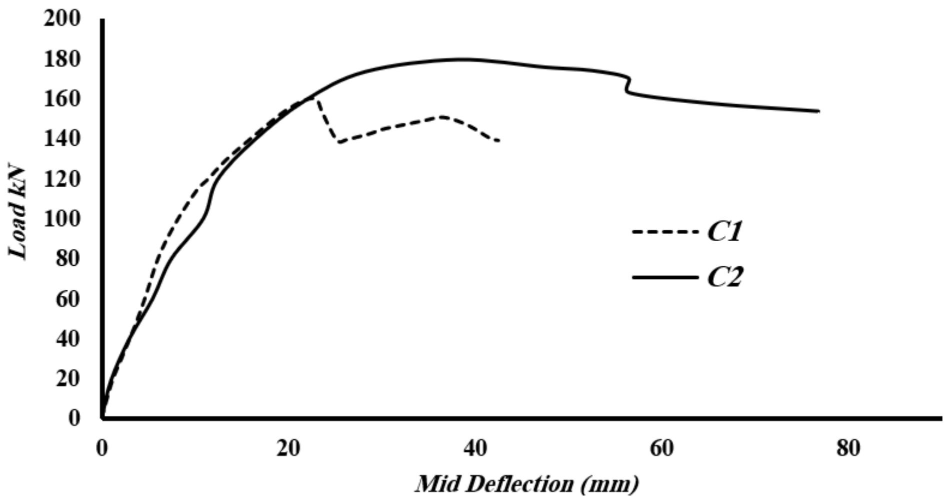

Fig. 2. Load-deflection response of Beams C1 and C2 used to illustrate variability in the composite beam response

Under the current level of applied load, when y maxL = i, the system is in state i. In the presence of increasing load, the system switches between discrete states, and the likelihood of these switches is determined by the transition probabilities, giving rise to probabilistic modeling frameworks [16]. In general, in a stochastic process, the probability of the system visiting a particular future state may not only depend on the current state but also on the whole sequence of earlier states (full history), and this is represented by the conditional probability of future states given the whole load–deflection history of the system

$$P[y_{max}(L_a) = j \colon y_{max}(L_{a-1}) = i, \dots . y_{max}(L_o) = 1] \tag{1}$$

Table 2. System state classification

State of the system	Implication	Mathematical representation
1	The maximum deflection is between y1 and y2	y1 < ymax ≤ y2
2	The maximum deflection is between y2 and y3	y2 < ymax ≤ y3
	.	
	.	
i	The maximum deflection is between yi and yi+1	yi < ymax ≤ yi+1
	.	
	.	
n	The maximum deflection is between yi and yi+1	yn < ymax

Let Z $(L^0, L^1, \dots, L_a^{-1}, L_a, \dots, L_m)$ represent the index set of the applied loads, and (1,2,..., i,j,...,n) represent the deflection statespace, which is the possible values of $[ymax(L), L \in Z]$ for each load La. The process of deflection goes through the intermediate state rules, which constitute the core modelling assumptions. The deflection process is modeled as a non-homogeneous Markov chain because the future value of the deflection only depends on the present value of the deflection. The non-homogeneity arises because the deflection transitions are associated with the different levels of load so that the discrete values index the process of the deflection $(L^1, L^0, \dots, L_N)$ of the levels of load, and a finite number of deflection states is assumed. The deflection is said to have N distinct values if it is categorized into N states, as shown in Table 2. Hence, the conditional transition probability of the deflection process is formulated appropriately as shown in equation (1).

$$PP_{ij}(L_{a-1}, L_a) = [y_{max(L_a)} = j \colon y_{max[\![(L)]\!]_{a-1})} = i]; \; L_{a-1} < \; L_a \tag{2}$$

The probability of the system transitioning from state i to state j under the load increment under the load of $La - 1 \; to \; La$. Let $P_{ij}(L_{a-1}, L_a)$ denote this transition probability. This probability captures the system's response as the applied load increases. The corresponding transition probability matrix, denoted by $[II(L_{a-1}, L_a)]$, defines the complete set of transition probabilities among n discrete states during the load increment or decrement from L_{a-1} to $, L_a$. As the load progresses, the loads are monotonically increasing. Thus, no transitions may occur between any of the lower deflection states. Consequently, the matrix will not include any entries below the diagonal (pij = 0) for rows above their column (i.e., for all j < i).

$$[II(L_{a-1}, L_a)] = \begin{array}{c} \\ 0 \\ 1 \\ 2 \\ 3 \\ 4 \\ 5 \\ . \\ n \end{array} \begin{array}{c} \begin{array}{cccccccc} 0 & 1 & 2 & 3 & 4 & 5 & . & n \end{array} \\ \begin{bmatrix} p_{00} & p_{01} & p_{02} & p_{03} & p_{04} & p_{05} & . & . \\ p_{10} & p_{11} & p_{12} & p_{13} & p_{14} & p_{15} & . & . \\ p_{20} & p_{21} & p_{22} & p_{23} & p_{24} & p_{25} & . & . \\ p_{30} & p_{31} & p_{32} & p_{33} & p_{34} & p_{35} & . & . \\ p_{40} & p_{41} & p_{42} & p_{43} & p_{44} & p_{45} & . & . \\ p_{50} & p_{51} & p_{52} & p_{53} & p_{54} & p_{55} & . & . \\ . & . & . & . & . & . & . & . \\ . & . & . & . & . & . & . & . \end{bmatrix} \end{array} \tag{3}$$

To make it easier to visually understand the suggested non-homogeneous Markov model, a state-transition diagram has been created (i.e., Figure 3). The seven deflection states are the nodes, while the arrows represent the feasible transition probabilities (pij) between the states. Since the primary loads applied to the beams are monotonically increasing, the transition from one downward state to another is irretrievable in the downward direction; thus, the only possible way for the system to remain in the same state or to go upward in deflection (but not downward). The final state is defined as the terminal high-deflection state.

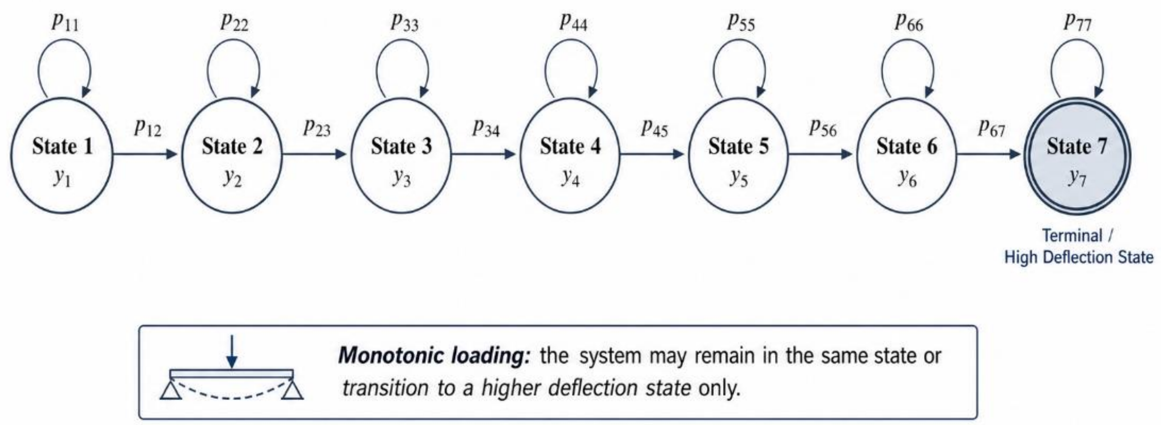

Fig. 3. Markov state-transition diagram for the seven deflection states under monotonic loading

The diagram includes State 1 through State 7, self-transition arrows pii, and forward transition arrows pij for j ≥ i. No backward arrows are shown because pij = 0 when j < i. Given that the deflection states defined in Table 2 are mutually exclusive and collectively exhaustive, the sum of each row in the transition probability matrix must equal one. As the load increases from (p_{00}), from $La - 1$ to La, the system's state, defined by the maximum deflection, can either remain unchanged or progress to a higher deflection level. A reversal to a lower deflection state is not possible. Consequently, the transition matrix reflects this non-decreasing behavior. To compute the transition probability Pij(L_{a-1}, L_a), it is necessary to consider both the marginal probability distribution of the maximum deflection at La-1 and La and the joint probability distribution of deflections at La-1 and La. Let Ma-1and Ma represent the maximum deflection at the respective load levels. Given the joint and individual probability density functions of these variables, the transition probability can be derived accordingly.

$$p_{12}\,(L_{a-1}, L_a) = \frac{\int_{y1}^{y2}\int_{y2}^{y3} f_{M_{a-1}.M_a}\,(M_{a-1}, M_a).\,dy_{a-1}.\,dy_a}{\int_{y1}^{y2} f_{M_{a-1}}\,(M_{a-1}).\,dy_{a-1}} \tag{4}$$

Let $f_{M_{a-1}.M_a}\,(M_{a-1}, M_a)$ denote the joint probability density function of the random variables Ma-1 and Ma, representing the maximum deflection at two successive load levels. Additionally, the marginal density function of $Ma - 1$ is denoted as $f_{M_{a-1}}\,(M_{a-1})$. It It is unrealistic to represent the behaviour of maximum deflection using an extreme-value distribution for Ma−1 and Ma, as previously described. It also will cause many difficult calculations. Calculating joint distributions, estimating parameters can be computationally challenging, especially when large experimental datasets are unavailable. For simplicity and computational feasibility, the individual and joint deflection variables were represented by normal and bivariate normal distributions, respectively, so that transition probabilities between consecutive deflection states could be determined from the mean deflection, standard deviation, and correlation coefficient as the loads were applied. While the present assumption is appropriate given the limitations of the current model as well as the smaller data set used to calibrate it, it does still constitute a form of modeling simplification. Since all deflection values are positive and may exhibit right-tailed skewness during advanced stiffness degradation, lognormal or other right-skewed distributions should be considered for future studies of future modeling studies with larger data sets. Thus the results from this model only relate to those tested beams which have been calibrated:

$$f_{M_{a-1}}\,(M_{a-1}) = \frac{1}{\sqrt{2\pi}.\,\sigma_{a-1}}.\,e^{-\left(\frac{1}{2}\right).\left[\frac{M_{a-1}-G_{a-1}}{\sigma_{a-1}}\right]^2} \tag{5}$$

$$f_{M_a}\,(M_a) = \frac{1}{\sqrt{2\pi}.\,\sigma_a}.\,e^{-\left(\frac{1}{2}\right).\left[\frac{M_a-G_a}{\sigma_a}\right]^2} \tag{6}$$

$$f_{M_{a-1}.M_a}\left(M_{a-1},M_a\right) = \frac{1}{2\pi.\sigma_{a-1}.\sigma_a.\sqrt{1-\rho^2}}.e^{-\left(\frac{1}{2.(1-\rho^2)}\right).\left\{\left[\frac{M_{a-1}-G_{a-1}}{\sigma_{a-1}}\right]^2-2\rho.\left[\frac{M_{a-1}-G_{a-1}}{\sigma_{a-1}}\right].\left[\frac{M_a-G_a}{\sigma_a}\right]+\left[\frac{M_a-G_a}{\sigma_a}\right]^2\right\}} \quad (7)$$

It can be assumed that the average max displacement measured at two sequential load levels, La-1 and La, denotes the respective mean values Ga and G_{a-1}. The measurements σ_{a-1} and σa will represent the respective standard deviations of the max displacement measured at La-1 and La. The correlation coefficient, ρ, denotes a statistical relationship established between the two maximum displacements measured at load levels La−1 and La.

In order to estimate the average deflection at a given loading level, the methodology combines the provisions of ACI 318 [17] and AISC 2016 [18]. Specifically, elastic analysis is applied to both uncracked and cracked transformed sections, as outlined in ACI 318-17. In contrast, the internal moment capacity of the composite section is determined using the plastic stress distribution concept described in AISC 2017. This combined approach enables enables accurately calculating mid-span deflection by accounting for both elastic and plastic behavior in steel–concrete composite sections.

$$y_{max} = \frac{p.(span)^3}{48.E_c.I_g} \qquad \textit{for the uncracked section} \quad (8)$$

$$y_{max} = \frac{p.(span)^3}{48.E_c.\left\{\left[\left(\frac{M_{cr}}{M_a}\right)^3.I_g\right]+\left[1-\left(\frac{M_{cr}}{M_a}\right)^3\right].I_{cr}\right\}} \qquad \textit{for the cracked section} \quad (9)$$

Where M_a, the moment at any applied load La, and M_{cr} is the moment at cracked load, I_g is the moments of inertia of the gross (Ig) and cracked (Icr) sections, respectively. The variable in the equation is the moment value at each point, and it will be in two forms, which are (M_{a-1}, M_a) and these equations yield two deflection values, which are $\left(y_{\max(a-1)}, y_{\max(a)}\right)$ used for training in addition to the values resulting from practical experiments.

The validation of the proposed Markov Framework is based on the defined training domain boundaries and state discretization employed. The Transition Probabilities considered were established from both the (i) Experimental Load-Deflection points obtained from testing, and (ii) Theoretical Response Points from the ACI318 and AISC provisions previously described in Section 3. Therefore, the application of the Markov Model to beams requires an alignment with the calibrated parameters of the training domain with regard to the section configuration (encased composite beams with embedded Steel I-sections), material classifications, reinforcement layouts, span-to-depth ratio, and Monotonic Load Protocol. Generalizing the model to new datasets outside of these parameters requires recalibration of the model. The discretisation of the deflections into a defined number of states will directly affect the smoothness and uncertainty of predictions; for example, if the state grid is coarse, the resolution for detecting changes in stiffness will be lower than that of a refined state grid. Conversely, if the state grid is refined, then the number of states will be high, resulting in sparse transition counts or unstable estimates. Therefore, state definitions were determined to provide an adequate number of samples per state to detect the primary curvature changes from the measured response. A sensitivity assessment of state size (number of deflection bins) is recommended when applying the model to new datasets, and the discretisation should be considered a fixed modelling parameter for each calibration set to which it is applied and should be reported as such.

4. Beam C1

To demonstrate the application of the proposed model, the analysis steps for Beam C1 are presented in detail, while Beam C2 is similarly evaluated, with only the final results reported. The specifications of Beam C1 have been previously outlined, and its corresponding load–deflection response is illustrated in Figure 4.

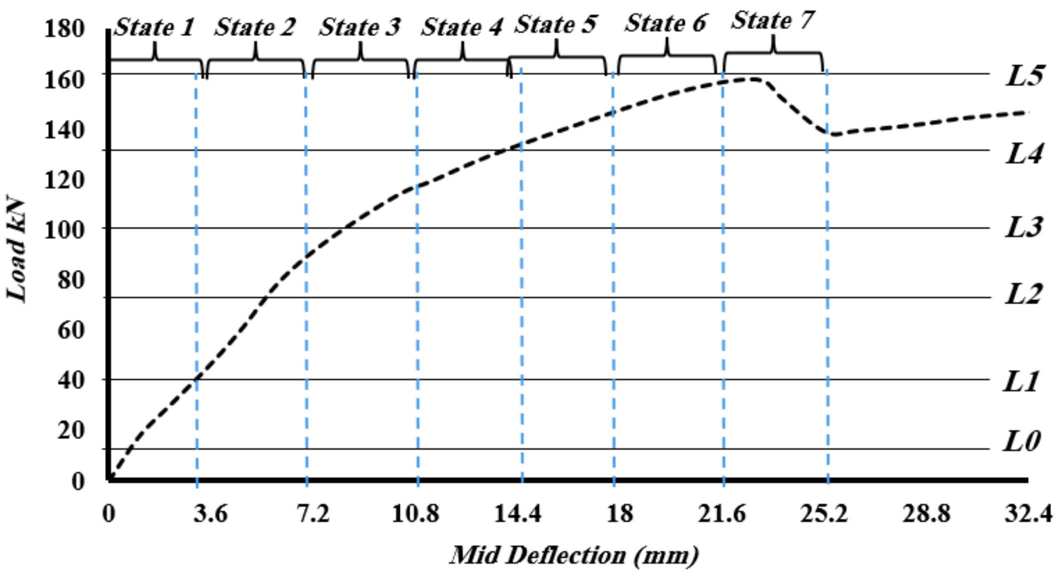

Fig. 4. Load deflection plot for beam C1

4.1 Step 1

In order to develop the transition probability matrix for the load–deflection behavior, it is necessary first to establish the index set, which represents discrete load levels, and the state space, which defines the corresponding deflection intervals. The index set captures the applied loads being stepped through, and the state space discretises the structural response into distinct deflection ranges [19]. These two combined form the basis for modeling a beam's behavior as a stochastic process with the Markov chain. For this application, the index set is broken up into discrete load levels 10, 40, 70, 100, 130, and 160 kN. The load points can be arbitrary as long as they fall within the range of interest and are suitable to capture the deflection progression during a load increase.

For the presented example, there are no specific rules guiding the choice of load points, and they do not have to meet any specific restrictions beyond spanning the range of interest, and should each correspond to a different measurable deflection state, except when multiple load levels induce the same deflection state.

- State 1: $0 < ymax < 3.6$ mm
- State 2: $3.6 < ymax < 7.2$ mm
- State 3: $7.2 < ymax \leq 10.8$ mm
- State 4: $10.8 < ymax \leq 14.4$ mm
- State 5: $14.4 < ymax \leq 18.0$ mm
- State 6: $18.0 < ymax \leq 21.6$ mm
- State 7: $ymax > 21.6$ mm

Table 3. The means and standard deviations of deflection at different loads of beam C1 (experimental and analysis data), assuming $\Omega = 0.25$

Load (kN)	Mean (mm)	Standard deviation (mm)
10	7.090	1.770
40	9.785	2.445
70	12.475	3.120
100	15.170	3.795
130	17.865	4.465
160	20.555	5.140

A framework that is achieved through the use of seven designated deflection states, which are mutually exclusive. In addition, the seven deflection states are constructed to be collectively exhaustive so that every possible structural response can be captured in one state, and so that each deflection value uniquely relates to one, and only one, possible outcome. Consequently, the load–deflection relationship can be effectively represented as a nonhomogeneous Markov chain, consisting of seven distinct deflection states and six discrete load levels: 10, 40, 70, 100, 130, and 160 kN. These six load levels produce five successive load intervals used to construct the transition probability matrices [20].

4.2 Step 2

To compute the transition probability matrices across successive load intervals, it is assumed that the deflection at any given load level Lk is a normally distributed random variable. Furthermore, the joint probability density of deflections at two consecutive load levels, Lk-1 and Lk, is modeled as a bivariate Gaussian distribution with an assumed correlation coefficient of 0.95 [11].

Equations 5–7 can be utilized to calculate the transition probabilities defined in Equation 3, provided that the relevant distribution parameters are known. While the mean deflections at load levels L_{k-1} and Lk are computed using Equations 8 and 9, the corresponding standard deviations were calculated using the adopted coefficient of variation (CV), as follows:

$$\sigma_{k-1} = CV \times G_{k-1} \tag{10}$$

$$\sigma_k = CV \times G_k \tag{11}$$

The values of G_{k-1} and G_k are the mean of the deflections representing two load levels, while σk−1 and σk represent the standard deviation of the respective mean deflection for the same two load levels. For this study, a coefficient of variation of (CV) of 0.25 was adopted based on the statistical analysis of available deflection data associated with Beams C1 and C2.

[II(L0,L1)] = (12)

0.325	0.657	0.018	0	0	0	0
0	0.19	0.739	0.071	0	0	0
0	0	0.147	0.6876	0.165	0.0004	0
0	0	0	0.085	0.6799	0.234	0.0011
0	0	0	0	0.0199	0.6891	0.291
0	0	0	0	0	0.0013	0.998
0	0	0	0	0	0	1

II(L1,L2)] = (13)

0.343	0.617	0.029	0.0111	0	0	0
0	0.256	0.673	0.066	0.005	0	0
0	0	0.221	0.647	0.131	0.0011	0
0	0	0	0.159	0.652	0.188	0.001
0	0	0	0	0.108	0.642	0.249
0	0	0	0	0	0.071	0.929
0	0	0	0	0	0	1.00

II(L2,L3)] = (14)

0.379	0.548	0.049	0.024	0	0	0
0	0.318	0.586	0.079	0.017	0	0
0	0	0.277	0.61	0.102	0.011	0
0	0	0	0.2197	0.6097	0.1622	0.0084
0	0	0	0	0.171	0.612	0.217
0	0	0	0	0	0.141	0.859
0	0	0	0	0	0	1

Simulations, which were based on the coefficient of variation, were used in lieu of a limited number of the available experimental deflection points. Statistical analysis performed on the available deflection data for Beams C1 and C2 produced coefficients of variation that ranged from approximately 0.16 to 0.25. The conservative coefficient of variation selected to estimate the maximum allowable is proposed to be used as a representative sample value (the upper limit). This selection was made due to the relatively high level of uncertainty that was associated with the limited amount of experimental data available, the presence of nonlinear reductions in stiffness, the continuing presence of cracks, and the variability of response from one specimen to another. Therefore, the $\Omega = 0.25$ coefficient of variation provides a conservative distribution for determining the transition probability matrices. The mean value as well as the standard deviation of the parameters for various load stages are exhibited in Table 3. Based on these values, transition probability matrices were created with regard to Equation 3 as well as Equations 5 to 7. The required integrals for Equation 3 were calculated using Gaussian quadrature, implemented in standard Python code from the NAG numerical library.

4.3 Step 3

By having the transition probability matrices for each load, we are now able to calculate multi-step transition probabilities. For example, the two-step transition matrix from L0 to L2 is obtained by multiplying the two consecutive one-step transition matrices:

$$[II(L_0, L_2)] = [II(L_0, L_1)]x\,[II(L_1, L_2)] \tag{15}$$

This notation indicates the probability of moving between deflection states from load level L0 to load level L2 through the intermediate load level L1. These calculations involve matrix multiplication of the transition probability matrices. The required transition probabilities were obtained using Gaussian quadrature, and the simulation program was implemented in standard Python, and the resulting matrix based on Eqs. 12 and 13 is:

[II(L0,L2)] (16)

0.111	0.369	0.456	0.059	0.006	0	0
0	0.049	0.291	0.502	0.144	0.014	0
0	0	0.032	0.204	0.486	0.235	0.042
0	0	0	0.014	0.129	0.469	0.388
0	0	0	0	0.002	0.062	0.936
0	0	0	0	0	0	1
0	0	0	0	0	0	1

Similarly, three-step, four-step, and five-step transition probability matrices are obtained.

4.4 Step 4

Since the calculated probabilities are conditional, determining the unconditional probabilities of the beam transitioning from the load level L_0 to L_2 requires first establishing the initial state distribution, In the initial state vector, the probabilities of the seven possible deflection states must sum to 1, not the probabilities of the load levels [21]. These initial probabilities act as the starting position for propagating probabilities across multiple load steps using the transition matrices. Figure 2 plots the experimental deflection data at the various loads from L_0, to L_5; deflections are clearly seen at each load. Deflection at intermediate loads is estimated through linear interpolation; it is now possible to observe the system at each load on the graph. The observed data show that the beam is in state 1 at L_0. The initial state probability vector is then:

$$[II(0)] = (1, 0, 0, 0, 0, 0, 0) \tag{17}$$

Table 4 demonstrates the unconditional probabilities based on the input load levels and was computed with equations (17) and the initial system probability vector, which was given in Equation [II(0)], shown in the last section. Additionally, to provide for a comparison, Table 4 also contains the corresponding deflection values from Figure 2. This analysis provides a probabilistic framework for evaluating of the structural response of Beam C1 as the load level is increased, based upon a correlation coefficient of p = 0.95.

Table 4. Unconditional probabilities of different states of beam C1 for p = 0.95

Increase in Load		Load step (m)	Vector	Unconditional Probabilities of Different States							Range of deflection having most significant probability of occurrence (mm)	Experimental deflection at load Lk (mm)
From Lk-1 (kN)	To Lk (kN)			1	2	3	4	5	6	7		
10	40	1	(IIU (L0,L1)]	0.325	0.657	0.018	0	0	0	0	3.6-7.2	3.05
10	70	2	(IIU (L0,L2)]	0.111	0.369	0.456	0.059	0.006	0	0	7.2-10.8	5.05
10	100	3	(IIU (L0,L3)]	0.013	0.065	0.189	0.291	0.273	0.128	0.041	10.8-14.4	8.02
10	130	4	(IIU (L0,L4)]	0.001	0.003	0.014	0.037	0.076	0.127	0.741	14.4-18	14.6
10	160	5	(IIU (L0,L5)]	0	0	0	0.001	0.002	0.005	0.992	18-21.6	22.6

- The sub-entry $P_{11(L_0,L_1)}$ represents, and it means the possibility that the system will stay at state 1 when the load changes from 10kN to 40kN. This value, 0.325, indicates a 32.5% likelihood that deflection remains within the 0–3.6 mm range at 40 kN, given it was within the same range at 10 kN. Other elements in the transition matrices $[II(L_0, L_1)]$, through $[II(L_1, L_2)], \dots, [II(L_4, L_5)]$follow similar interpretations. Notably, state 7 serves as the absorbing state in all matrices. An examination of Equations 10–12 reveals a consistent decline in the diagonal and first super-diagonal probabilities as the load increases from (L_0, L_1) to (L_1, L_2) and (L_2, L_3). This is the the trend in deflection magnitude in the deflection between any subsequent load steps not linked with a change in direction of applied load.
- The first element of the two-step transition probability matrix $II(L_0, L_2)$, specifically $p_{11(L_0,L_2)}$, is calculated to be 0.111. This indicates that, starting in state 1 at a load of 10 kN, there is an 11.1% probability that the system remains in state 1 when the load reaches 70 kN. In other words, the likelihood of deflection staying within the 0–3.6 mm range under this load increase is relatively low. Multi-step transition probability matrices such as this are effective methods for estimating deflection at elevated load levels based on deflection observations at earlier stages.
- Assuming the system initially occupies state 1, the unconditional probabilities corresponding to each state at successive load levels are computed as part of Step 4. The resulting probability vector $[II(L_0, L_2)]$ reflects the likelihood of the system being in each possible state at load L_2, given it began in state 1 at L_0, as described by Equation 15.
- As shown in Table 4, the model estimates that at 40 kN, the beam will be in state 1 with 32.5% probability, state 2 with 65.7%, and state 3 with 1.8%, based on the initial state vector from Equation 15. The table also highlights, for each load increment, the most probable state. At 40 kN (after the first load step), the most likely deflection range is 0–3.6 mm, which aligns well with the observed deflection of 3.05 mm from Figure 2. This indicates good model accuracy at early stages. Similarly, the model's prediction remains consistent at 70 kN (second load step), though it forecasts a higher likelihood (29.1%) for state 3 (10.8–14.4 mm), while the actual deflection was only 3.02 mm. The states predicted at the higher levels of loading (130kN and 160kN) were slightly less than what was experimentally measured for the same load levels. Specifically, for 130kN, the 14.4-18.0mm range was predicted, while the measured deflection was measured to be 14.6mm which was at the lower bound of the same non-linear transition range. Then, at 160kN, the measured deflection was 22.6mm and well above its predicted value of 18.0-21.6mm. The difference indicates that at this load level the beam had begun to respond much more strongly in a non-linear way; i.e. cracking formation, stiffness degradation and re-distribution of internal forces were increasingly pronounced. The differences are also indicative of the fact that, using a Markov-chain methodology, there

is a non-homogeneous nature in the transitions as a result of large load levels, and therefore the probability of moving from one deflection state to another changes as a result of the load level – therefore the difference at the higher load levels represents an inadequacy of using fixed intervals between deflection states and/or assuming a normal transition during advanced non-linear behaviour.

5. Beam C2

In addition to Beam C1, Beam C2 was also analysed following the methodology established for Beam C1, and only the final results for Beam C2 are presented herein. Beam C2 specifications are, as already defined, and the load-deflection response for Beam C2 is illustrated in Figure 5.

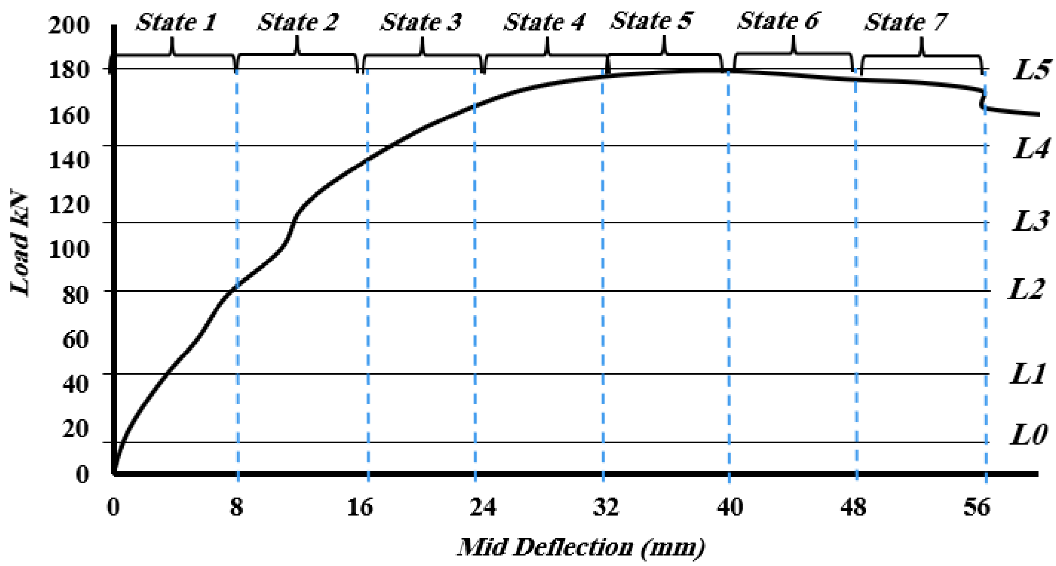

Fig. 5. Load- deflection plot for beam C2

Table 5. Unconditional Probabilities of Different States of Beam C2 for ρ = 0.95.

Increase in Load From Lk-1 (kN)	Increase in Load To Lk (kN)	Load step (m)	Vector	Unconditional Probabilities of Different States 1	2	3	4	5	6	7	Range of deflection having the most significant probability of occurrence (mm)	Experimental deflection at load Lk (mm)
13	44	1	(IIU (L0,L1)]	0.098	0.368	0.513	0.018	0.002	0.000	0.000	0-8	4.53
13	81	2	(IIU (L0,L2)]	0.031	0.152	0.389	0.345	0.078	0.005	0.000	16-24	8.03
13	110	3	(IIU (L0,L3)]	0.010	0.056	0.199	0.302	0.305	0.108	0.021	24-32	12.4
13	145	4	(IIU (L0,L4)]	0.003	0.019	0.085	0.170	0.277	0.255	0.191	32-40	18.3
13	180	5	(IIU (L0,L5)]	0.098	0.003	0.011	0.018	0.368	0.513	0.000	40-48	38.6

Table 5 lists the results of the revised C2 deflection-state intervals for compatibility with the current loading progressions, and will display continuous state definitions starting from the first state defined as 0-8 mm of deflection. The results display good correspondence between the overall trend of deflection (increase) as a load increases, but do not correspond consistently with the amount of deflection shown at each load. At 44 kN, the measured deflection (4.53 mm) falls into state 1; consequently, the higher predicted probability of being in the upper state compared to the coefficient of variation used in the calculation, indicates that the increased variance of the probability distribution associated with the normal transition rule would yield a higher state assignment when applied to the first loading period (44 kN). At 180 kN, the measured deflection (38.6 mm) lies in the 32-40 mm interval and in contrast, the most probable interval given the

Markov process would provide a predicted maximum deflection at 40-48 mm. Additionally, using only a fixed number of deflections for determining states results in an overestimator for the predicted maximum deflection and emphasizes the influence of the non-linear change in stiffness and lack of resolution associated with each state suggesting that the C2 results primarily follow the general trend rather than providing exact state-by-state predictions rather than specifying an exact state-by-state prediction[21]. This can help in predicting the behavior of reinforced concrete beams under monotonic increasing loads through a non-homogeneous Markov model, where the consecutive deflection variables Ma−1 and Ma are assumed to be bivariate normally distributed with a correlation coefficient ρ = 0.95.

Many current codes provide recommendations on detailing practices to limit deflection, and some also provide procedures to estimate deflection under service loads. The probabilistic framework that is presented herein is an alternative to these codes. It is a statistically based methodology that allows the determination of deflection, taking into account a validated elastic deflection calculation method (with some accuracy). This model allows the user to estimate the deflection likely to be reached at higher load levels, given the response at a lower load stage. This is particularly useful when trying to assess beam behavior under potential overloading scenarios, especially when deflections approach or exceed serviceability limit states.

6. Predictive Performance

In order to objectively assess the predictive performance of the proposed non-linear Markov model (NLMM), load-deflection predictions from the model were compared with experimental responses from Beams C1 and C2, which were used as the benchmark datasets. Model accuracy was quantified at matched load levels using six commonly accepted statistical indicators: root mean square error (RMSE), normalized root mean square error (NRMSE), mean absolute percentage error (MAPE), accuracy acceptance (AA), coefficient of determination (R^2), and Pearson's correlation coefficient (R). The purpose of these indicators is to provide complementary information related to the model's predictive accuracy: RMSE emphasizes large deviations, NRMSE allows for a scale-independent comparison of the two beams, MAPE and AA provide relative error reported as a percentage, and R^2 and R describe the strength of linear correlation between the predicted and measured responses. Together, these indicators provide an objective and reproducible quantitative assessment of the predictive performance of the proposed Markov model. Equations (18)-(22) were used to compute the values of the six statistical indicators evaluated in this study. This study used the following definitions: N=number of pairs of Measured-Predicted deflections, An= measured deflection at Load Level n, Pn= predicted value as obtained from the Newly Proposed Markov Model at Load Level n, and Ā=Average of the Measured Deflections. Thus, all Statistical Indicators utilized paired Measured and Predicted Deflections on Beams C1 & C2. The statistical indicators, including RMSE, NRMSE, R^2, MAPE, and AA, were calculated as follows:

$$RMSE = \sqrt{\frac{1}{N}\sum_{n=1}^{N} (A_n - P_n)^2} \tag{18}$$

$$NRMSE = \frac{RMSE}{S} \tag{19}$$

$$R^2 = 1 - \frac{\sum(A_n - P_n)^2}{\sum(A_n - \bar{A})^2} \tag{20}$$

$$MAPE = \frac{\left(\sum\frac{|A_n - P_n|}{A_n}\right) * 100}{N} \tag{21}$$

$$AA\,\% = 100\,\% - MAPE \tag{22}$$

Where S is the range of the measured deflection values and is calculated as S = Amax − Amin. Here, Amax and Amin are the maximum and minimum measured deflections, respectively, Ā is the mean of the measured deflection values. Pearson's R was computed using the standard correlation formulation between An and Pn. Notation was kept consistent across beams, and all metrics were computed from the same paired datasets to ensure comparability.

Table 6. Statistical performance evaluation of the experimental results and the Markov model

Beam	RMSE (mm)	NRMSE	MAPE (%)	AA% (%)	R^2	Pearson R
Beam C1	3.0252	0.0236	2.36	97.62	0.9920	0.9931
Beam C2	6.6379	0.0483	6.91	93.03	0.9783	0.9906

Table 6 lists the values of the indicators for both beams. The absolute error for Beam C1 produced by the Markov model was low (RMSE = 3.03 mm; NRMSE = 0.0236), producing a very low MAPE of 2.36% (AA = 97.62%). The strong correlation and goodness-of-fit (R^2=0.9920, R=0.9931) between the two data sets indicate that the model replicated the entire non-linear evolution of the experimental response at a high degree of accuracy. In contrast, the absolute and relative errors for Beam C2 were higher than those produced by Beam C1 (RMSE = 6.64 mm; NRMSE = 0.0483; MAPE = 6.91%; AA = 93.03%); however, the correlation metrics remained at a relatively high level (R^2=0.9783, R=0.9906). This suggests that the model was still able to track the trend and monotonic progression of the response; however, the discrepancies in pointwise comparison of the two beams had become larger. The larger pointwise discrepancies for Beam C2 correspond to the increased degree of complexity in Beam C2's stiffness degradation and transitional behavior, where local cracking progression and interactions between materials may exist such that they produce greater curvature changes that may be difficult to capture accurately using a finite-state structure.

The quantitative interpretation of the predictions for both configurations also allows for additional understanding via a comparative analysis between the predicted results of C1 (3.03 mm RMSE) and C2 (6.64 mm RMSE), in addition to the qualitative (overlay of curves). The increase in the RMSE value from C1 to C2 (e.g., 3.03 kN to 6.64 kN) indicates that in C2, the larger predictions tended to occur more frequently and/or at a greater magnitude than in C1. The greater NRMSE and MAPE values in C2 also indicate that the lack of accuracy from C1 to C2 is not solely due to scaling but reflects an increase in the relative amount of prediction errors. The consistently high Pearson R values (> 0.99) between both tests show that the Markov predictive model preserved the appropriate monotonic ordering and the overall response shape; as such, the errors were primarily due to localized increases in the prediction error. Ultimately, the decrease of the R^2 value (0.9920 for C1 to 0.9783 for C2) suggests that although the measurement data still contained large localized amounts of nonlinearity, the proportion of variance accounted for still experienced a slight reduction. Collectively, these quantitative results indicate that the proposed predictive model provides an accurate and statistically demonstrable way to predict the monotonic load-deflection response and provides an objective basis for a performance comparison of the alternate beam systems.

To facilitate a better visual interpretation of the numerical outcomes listed in Tables 4 and 5, Figures were added to compare the Beams C1 and C2 experimentally with their respective Markov predictions. In Figure (6); the experimental deflection data points of Beam C1 are plotted against the Markov prediction of their most probable deflection interval for each of the specified loading levels (or steps). Figure (6) displays a similar comparison for Beam C2. For both beams, the experimental deflection data points are displayed alongside the probability band/error bar of the most likely State of Deflection according to Markov; therefore visually showing the deviations from the Markov prediction associated with each level of Loading deformation applied.

Overall, the graphical comparison for Beam C1 shows that experimental deflection tends to match the anticipated state transition with increasing deviation towards the final loading stage; however, for Beam C2 there is an obvious and significant difference between measured and predicted deflection states at 180kN, with measured deflection being measured as 38.6mm compared to predicted range of 40-48mm. The model indicates a slight overestimation of the final deflection state of Beam C2 based on fixed increment discrete state representation and stronger nonlinear stiffness reduction at higher levels of load.

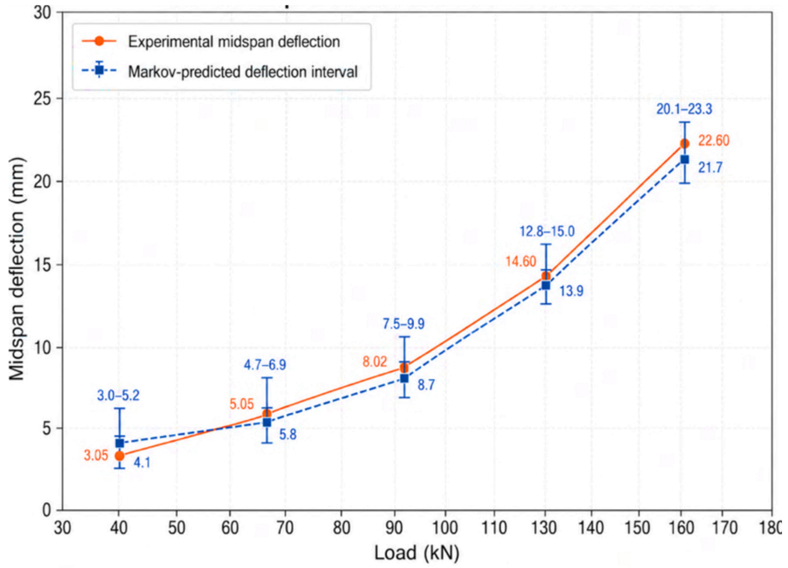

(a)

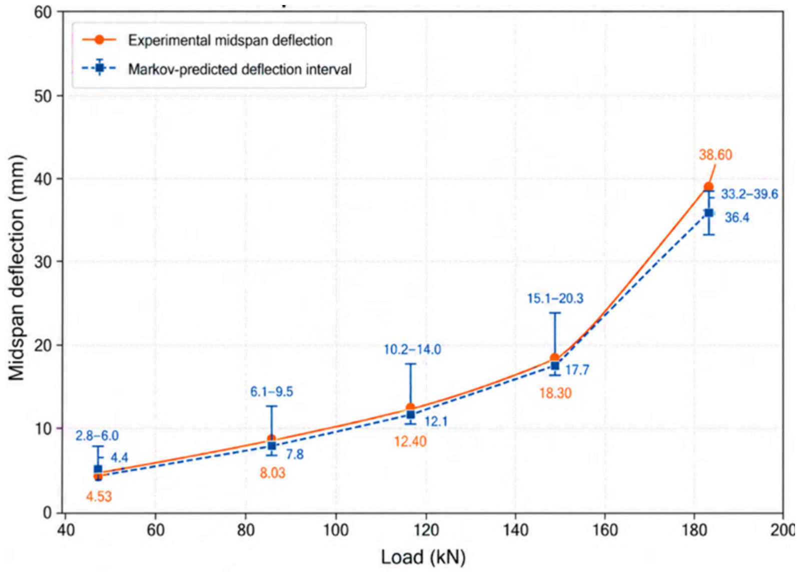

(b)

Fig. 6. Graphical comparison between experimental deflection and Markov-predicted deflection interval for: (a)- Beam C1, (b)- Beam C2

For the quantitative evaluation of each Markov model's ability to predict deflection, multiple metrics were used: RMSE, NRMSE, MAPE, AA, R^2 and Pearson R. Each metric provides a basis for the predicted deflection states can be compared to the experimental deflections for Beams C1 and C2. As previously reported in Tables 4 and 5, predicted deflection intervals that corresponded to each experimental deflection value were identified, while Table 6 presented all statistical evaluations. Therefore. The parameters specified here are to be understood by reference to the assumptions used for this model: first, transition probabilities were obtained using a normal distribution assumption; second, fixed deflection-state intervals were defined; third, each of the experimental load and deflection measurements was taken at only a limited number of load-deflection points; and lastly, certain loads required interpolation for estimation. Therefore, the performance metrics obtained and communicated in this report reflect the ability to follow trends rather than providing absolute predictive accuracy over the entire range of loading conditions.

7. Conclusions

This research establishes and assesses a non-homogenous Markov chain method for predicting the load-deflection response of concrete-encased steel I-beams under monotonic three-point bending.

Structural response is defined as a series of discrete deflection states corresponding to increasing loads, rather than a single deterministic load-deflection curve. Through combining transition probabilities and response estimates based on the American Concrete Institute (ACI) and the American Institute of Steel Construction (AISC) calculations, a simplified probabilistic model can be used to track the degradation of stiffness and deflection of composite steel-concrete beam systems over time.

The study concluded that the Markov approach can follow approximate experimental values for the load-deflection performance of Beam C1 and Beam C2. Specifically, the RMSE of 3.03 mm, AA of 97.62%, and R^2 of 0.9920 indicated a high correlation with the experimental results for beam C1, while the RMSE of 6.64 mm, AA of 93.03%, and R^2 of 0.9783 showed some correlation with the experimental values for Beam C2. There was a significant overestimation of the deflection response of Beam C2 at the last level of applied load, which suggests that the accuracy of the model is dependent upon the selected deflection-state intervals and the amount of nonlinear degradation of stiffness due to high levels of applied load.

This research provides a new approach to modelling the load-deflection behaviour of concrete-encased steel I-beams by using a Markov chain based probabilistic model. Traditional deterministic models provide a single predicted curve, while the proposed Markov chain model estimates the probability of transition between deflection states as load increases. This provides more information about the uncertainty in a structure’s behaviour and can aid in determining serviceability of composite beams. However, this study's model should only be applied within the calibrated range of specimens studied, and further validation should be performed prior to application to different geometry beams, loading protocols, or composite sections.

Future research is needed to confirm the proposed Markov model by utilising a larger sample of concrete-encased steel beam specimens of differing spans/reinforcements/materials/reinforcement spacing and concrete strengths. Other research efforts should explore how varying the size of the intervals/states, load/steps and correlation coefficient (ρ) will affect the stability of the transition probabilities. Additionally, expanding this model to other load protocols (e.g., repeated, cyclic and long-term) will provide further insight into the general utility of serviceability prediction analysis for composite beams.

References

[1] Bai H, Xu J, Demartino C, Zhao X. Probabilistic code-based shear capacity model for I-shaped steel reinforced concrete (SRC) beams. Engineering Structures. 2024;301:117180. https://doi.org/10.1016/j.engstruct.2023.117180

[2] Abdullatef A D, Ali S I, Aldarraji S Y H, Ali M I. Evaluating the Ramberg–Osgood Model for nonlinear moment–curvature analysis of reinforced concrete beams. Res. Eng. Struct. Mater., 2026; 12(2): 1165-1177. http://dx.doi.org/10.17515/resm2026-1518st0217rs

[3] Yu Y, Xie T, Xu J, Lai Z, Elchalakani M. Probabilistic models for characteristic bond stresses of steel-concrete in steel reinforced concrete structures. Engineering Structures. 2024;300:117167. https://doi.org/10.1016/j.engstruct.2023.117167

[4] Ahmed AM, Ali SI, Ali MI, Jamel AAJ. Analyzing Self-Compacted Mortar Improved by Carbon Fiber Using Artificial Neural Networks. Matrix. 2023;9:11. https://doi.org/10.18280/acsm.470602

[5] Alkayem NF, Shen L, Mayya A, Asteris PG, Fu R, Di Luzio G, et al. Prediction of concrete and FRC properties at high temperature using machine and deep learning: a review of recent advances and future perspectives. Journal of Building Engineering. 2024;83:108369. https://doi.org/10.1016/j.jobe.2023.108369

[6] Jabbar AA, Irzooki RH, Al-Obaidi AA. Improving resistance of gravity dam to seismic wave by using stepped base. In: E3S Web of Conferences. EDP Sciences; 2021. p. 01007. https://doi.org/10.1051/e3sconf/202131801007

[7] Richard D, Hong T, Hastak M, Mirmiran A, Salem O. Life-cycle performance model for composites in construction. Composites Part B: Engineering. 2007;38(2):236-246. https://doi.org/10.1016/j.compositesb.2006.04.001

[8] Ali MI, Allawi AA. An Artificial Neural Network Prediction Model of GFRP Residual Tensile Strength. Engineering, Technology & Applied Science Research. 2024;14(6):18277-18282. https://doi.org/10.48084/etasr.9107

[9] Loebens N, de Andrade Porto JV, de Andrade Porto KR, Souza JS, Pistori H. Types of Markov random fields in deep learning: A review. Neurocomputing. 2025:132353. https://doi.org/10.1016/j.neucom.2025.132353

[10] Ortner R. An identity for the bias in Markov reward processes with applications to Markov chain perturbation and Kemeny's constant. Statistics & Probability Letters. 2025:110592. https://doi.org/10.1016/j.spl.2025.110592

[11] Feng M, Pi B, Deng LJ, Kurths J. An evolutionary game with the game transitions based on the Markov process. IEEE Transactions on Systems, Man, and Cybernetics: Systems. 2023;54(1):609-621. https://doi.org/10.1109/TSMC.2023.3315963

[12] Mousavirad SJ, Ebrahimpour-Komleh H, Schaefer G. Convergence Analysis of the Human Mental Search Algorithm by a Markov Model. Knowledge-Based Systems. 2025:115073. https://doi.org/10.1016/j.knosys.2025.115073

[13] Geiger BC. Information-theoretic reduction of Markov chains. arXiv preprint arXiv:2204.13896. 2022.

[14] Xian G, Zhang Y, Wang Y. Experimental study on the flexural behavior of steel-concrete composite beams. Journal of Constructional Steel Research. 2012;77:59-67.

[15] Mahmood EM, Ibrahim TH, Allawi AA, El-Zohairy A. Experimental and numerical behavior of encased pultruded GFRP beams under elevated and ambient temperatures. Fire. 2023;6(5):212. https://doi.org/10.3390/fire6050212

[16] Watson SR. Probability Concepts in Engineering Planning and Design Vol 1-Basic Principles. AH-S. Ang and WH Tang. Wiley, New York. 1975;79(779):518-518. https://doi.org/10.1017/S0001924000036162

[17] American Concrete Institute (ACI). Building Code Requirements for Structural Concrete (ACI 318-17) and Commentary. Farmington Hills, MI: ACI; 2017.

[18] American Institute of Steel Construction (AISC). Steel Construction Manual. 15th ed. Chicago, IL: AISC; 2017.

[19] Zhao P, Kang Y, Niu B, Song X. Stochastic stability of positive Markov jump sub-homogeneous and homogeneous non-linear systems. Automatica. 2026;184:112730. https://doi.org/10.1016/j.automatica.2025.112730

[20] Basnarkov L. Semi-Markov random walk on complex networks. Chaos, Solitons & Fractals. 2026;202:117578. https://doi.org/10.1016/j.chaos.2025.117578

[21] İzgi B, Özkaya M, Üre NK, Perc M. Machine learning tree trimming for faster Markov reward game solutions. Journal of Computational Science. 2025:102726. https://doi.org/10.1016/j.jocs.2025.102726